The Astrophysical Journal Letters, 902:L42 (10pp), 2020 October 20 https://doi.org/10.3847/2041-8213/abbfb8

Stringent Search for Precursor Emission in Short GRBs from Fermi/GBM Data and Physical Implications

Jie-Shuang Wang[1], Zong-Kai Peng[2,3], Jin-Hang Zou[2,3], Bin-Bin Zhang[2,3,4], and Bing Zhang[4]
[1] Tsung-Dao Lee Institute, Shanghai Jiao Tong University, Shanghai 200240, People's Republic of China; jiesh.wang@gmail.com
[2] School of Astronomy and Space Science, Nanjing University, Nanjing 210093, People's Republic of China
[3] Key Laboratory of Modern Astronomy and Astrophysics (Nanjing University), Ministry of Education, People's Republic of China
[4] Department of Physics and Astronomy, University of Nevada Las Vegas, NV 89154, USA; bbzhang@nju.edu.cn
Received 2020 July 31; revised 2020 September 28; accepted 2020 October 9; published 2020 October 21

Abstract

We perform a stringent search for precursor emission of short gamma-ray bursts (SGRBs) from the Fermi/GBM data and find 16 precursor events with $\gtrsim 4.5\sigma$ significance. We find that the durations of the main SGRB emission ($T_{\rm GRB}$) and the precursor emission ($T_{\rm pre}$), as well as the waiting time ($T_{\rm wt}$) in between, are roughly comparable to each other, with $T_{\rm wt} \approx 2.8\ T_{\rm GRB}^{1.2}$ approximately satisfied for most cases except one significant outlier. We also perform spectral analyses to the precursors and SGRBs, and find that the spectra of precursor emission can be fitted with the blackbody, nonthermal cutoff power law and/or power-law models. We consider several possible models for precursor emission in SGRBs and find that the luminosity and spectral shape may be explained by the the shock breakout or the photospheric radiation of a fireball launched after the merger for thermal precursors, or magnetospheric interaction between two neutron stars prior to the merger for nonthermal precursors. For the fireball photospheric model, a matter-dominated jet is preferred and a constraint on the fireball Lorentz factor can be placed as $\Gamma \sim 30$. For the magnetospheric interaction model, the jet launching mechanism may be constrained. In particular, those events with $T_{\rm wt}/T_{\rm GRB} \gg 1$ (e.g., GRB191221802) require the formation of a supramassive or stable neutron star after the merger, with the delay time defined by the timescale for an initially baryon-loaded jet to become magnetically dominated and relativistic.

Unified Astronomy Thesaurus concepts: Gamma-ray bursts (629); Neutron stars (1108); Gravitational waves (678); Astrostatistics (1882)

1. Introduction

The joint detection of a gravitational-wave (GW) event GW170817 and a short gamma-ray burst (SGRB) GRB 170817A confirms that at least some SGRBs originate from double neutron star (NS) mergers (Abbott et al. 2017a, 2017b; Goldstein et al. 2017; Zhang et al. 2018b). Later, another NS merger event, GW190425, was discovered (Abbott et al. 2020), and a subthreshold GRB, GBM-190816, was reported to be possibly associated with a subthreshold GW event (Goldstein et al. 2019; Yang et al. 2020). While the GW observations alone can provide constraints on the NS equation of state (e.g., Abbott et al. 2017a, 2020), the joint GW–electromagnetic (EM) detections would provide further useful information about the physics of NS mergers and associated GRBs, including the jet launching mechanism, jet structure, jet composition, as well as the GRB radiation mechanism (e.g., Troja et al. 2017, 2019; Mooley et al. 2018a, 2018b; Zhang et al. 2018b; Geng et al. 2019; Gill et al. 2019; Zhang 2019; Ryan et al. 2020; Yang et al. 2020).

Copious EM signals are expected to be generated before and after the NS merger (for reviews, see Berger 2014; Fernández & Metzger 2016; Zhang 2018; Metzger 2019). Prior to the merger, EM signals can be produced by the interaction between the magnetospheres of the two NSs (Hansen & Lyutikov 2001; Lai 2012; Palenzuela et al. 2013; Wang et al. 2016, 2018b) or possible crust cracking of one or both NSs (Tsang et al. 2012; Suvorov & Kokkotas 2020). These mechanisms can lead to gamma-ray signals, which could be observed as precursor emission of SGRBs (e.g., Troja et al. 2010; Wang et al. 2018b). Precursor emission of SGRBs can also be produced after the merger. If the main SGRB emission is produced by the standard GRB mechanism (e.g., synchrotron radiation in an internal shock or magnetic dissipation site), a thermal precursor may be produced either as the shock breaks out from the surrounding ejecta or as the fireball ejecta reaches its photosphere radius (e.g., Mészáros & Rees 2000; Ramirez-Ruiz et al. 2002).

Many efforts have been made to search for precursor emission for GRBs. Precursors were first identified in long GRBs (e.g., Lazzati 2005; Burlon et al. 2008, 2009; Hu et al. 2014; Zhang et al. 2018a). For NS-merger-origin SGRBs, intense, short γ-ray emission is expected to occur shortly after the merger. The detection of precursor emission is therefore of great interest to diagnose the physical process right before or shortly after the merger. Observationally, identifying a weak signal before the main SGRB signal often suffers from instrumental biases, such as the energy range and sensitivity. The Fermi/Gamma-ray Burst Monitor (GBM) covers a broad energy band (from ~8 keV to 40 MeV), while the Swift/Burst Alert Telescope (BAT) is more sensitive in the 15–150 keV range. Thus, Swift/BAT would have a higher rate to detect soft weak precursors. Indeed, Troja et al. (2010) found that ~8%–10% SGRBs detected by Swift/BAT are associated with precursor activities, while in the SPI-ACS/INTEGRAL SGRB catalog, only <0.4% of the SGRBs are found to have precursor emission (Minaev & Pozanenko 2017).[5] Recently,

[5] One event, GRB 100717, was actually regarded as a long GRB in the Fermi/GBM catalog. However, Wang et al. (2018b) analyzed the spectra of GRB 100717 and found that this event can be well explained as an SGRB with a precursor generated by magnetospheric interaction between two merging NSs.

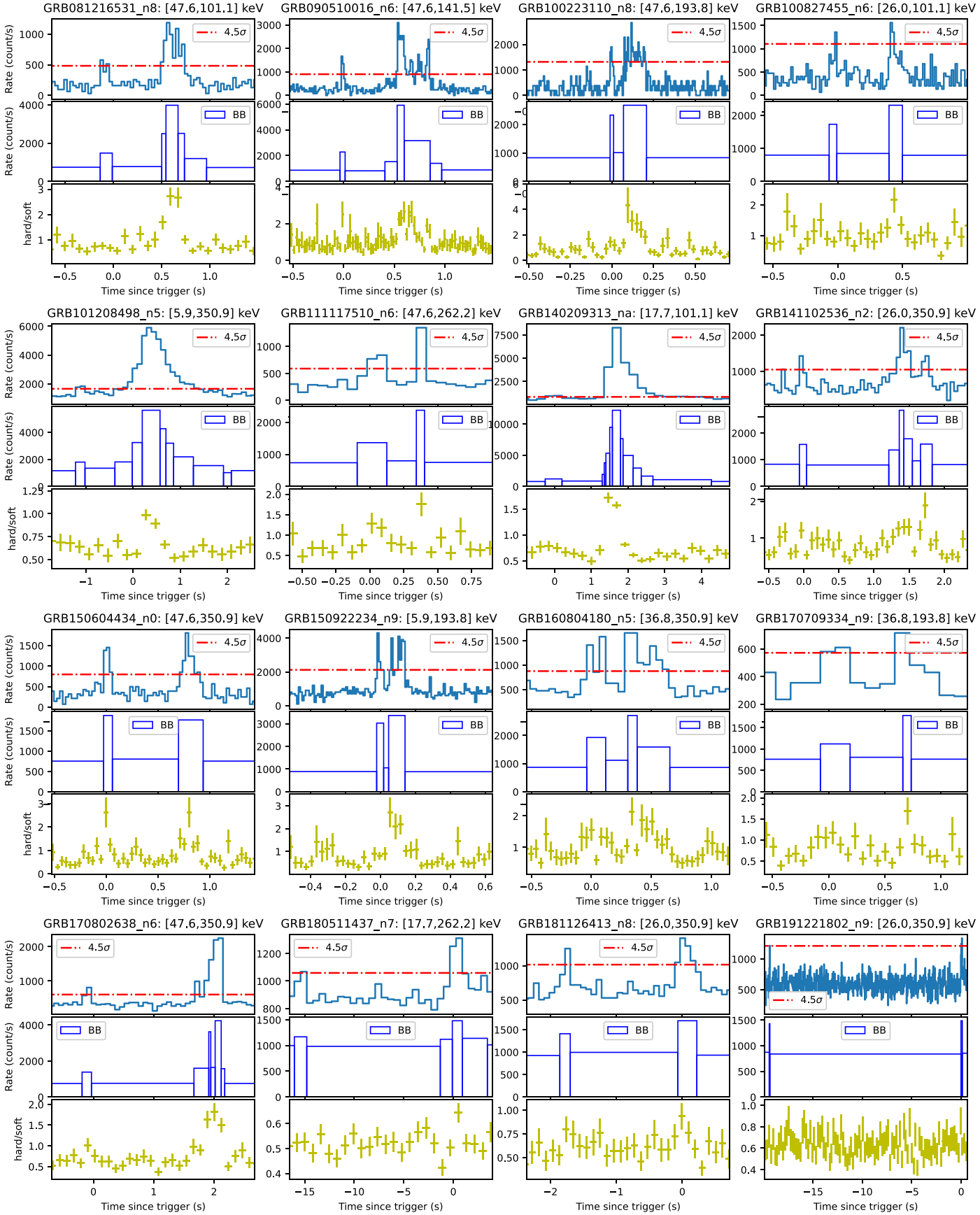

Figure 1. The light curves of SGRBs from the NaI detector with the highest significance for their precursors. We use both the traditional histogram and BB algorithm. The traditional histograms are obtained for the specific energy range optimized for the significance level of the precursor. Note that for GRB150922234, the peak flux of the precursor appears larger than that of the main pulse, but it is smaller than in the light curve of the full energy band (and hence is defined as precursor emission). The hardness ratio (hard/soft) is the ratio of numbers between hard photons (50–800 keV) and soft photons (10–50 keV).

Zhong et al. (2019) analyzed the Swift and Fermi/GBM SGRB data and found that 2.7% of SGRBs have precursor emission.

In this Letter, we study the precursor emission of SGRBs in detail both observationally and theoretically. In Section 2, we first perform a systematic search for precursors in the Fermi/GBM SGRB catalog and then perform detailed data analyses to extract the temporal and spectral information of both the precursor and the main SGRB emission. In Section 3, we discuss the validity of several precursor models and constrain these models using observations. The conclusion and discussion are presented in Section 4.

2. Data Analysis and Results

2.1. Precursor Emission in Fermi/GBM SGRB Sample

SGRBs are usually classified based on the duration criterion $T_{90} \lesssim 2$ s. However, since the duration of GRB 170817A (associated with GW170817) is 2.05 s (Zhang et al. 2018b), in this Letter we adopt a more conservative criterion $T_{90} \lesssim 3$ s to identify SGRB candidates. Up to 2020 April, Fermi/GBM detected 529 such SGRB candidates (Narayana Bhat et al. 2016; see also the online catalog[6]). GBM consists of 12 sodium iodide (NaI) detectors (sensitive to the 8 keV–MeV band) pointing to different directions and two bismuth germanate (BGO) detectors (sensitive to the 200 keV–40 MeV band). We sort out two NaI detectors that have the smallest angular separations with respect to the sky position of the corresponding GRB. The Time-Tagged Event data from the two NaI detectors are used to construct the light curve, which provide the arrival times and photon energies. We select the data with a photon arrival time between $T_0 - 50$ s and $T_0 + 30$ s, where T_0 is the GRB trigger time. Using the Bayesian Block (BB) algorithm (Scargle et al. 2013) in the Astropy package (Astropy Collaboration et al. 2018), we segment the photons into a sequence of time blocks, as shown in Figure 1. We then search for precursor emission in these time-block sequences.

A precursor is defined as the first pulse in the light curve. It must satisfy the following three requirements: (1) the peak flux is lower than that of the main pulse; (2) the flux during the waiting time period (the time interval between the precursor and the main pulse) is consistent with the background level; (3) the significance level is larger than 3σ. The first two requirements are the common definitions to identify precursor emission in SGRBs. The last one is reinforced in our study to reduce false-alarm signals. The second or main pulse is regarded as the main SGRB. To further strengthen the connection between the SGRB and the precursor, we also examined whether the precursor emission is only significant in the detectors in which the main pulse is bright. Then we follow the common definition of T_{90} to calculate the durations of the precursor emission ($T_{\rm pre}$) and the main SGRB ($T_{\rm GRB}$), as well as the waiting time ($T_{\rm wt}$) in between. The significance level of the precursor depends on time-bin size, energy band, and the background level. We take the background data from two time intervals, i.e., 30 s before the precursor and 30 s after the main SGRB. We then simultaneously vary the energy band and bin size (limited to $<0.5\ T_{\rm pre}$) to determine the maximum significance level.

[6] https://heasarc.gsfc.nasa.gov/W3Browse/fermi/fermigbrst.html

2.2. Properties of the Precursor and the Main SGRB Emission

Using the above three requirements, we identify 16 precursor events of SGRBs in the Fermi/GBM catalog, accounting for 3.0% of the full sample. Albeit we set 3σ as the threshold, we find the significance level of our precursor sample satisfies $\gtrsim 4.5\sigma$. The light curves of these SGRBs using both the ordinary histograms and BB algorithms, as well as the evolution of the hardness ratio, are shown in Figure 1. To further study their spectral properties, we employ the McSpecFit package (Zhang et al. 2018a) to perform the spectral fitting for the precursor and main SGRB emission components using the data from two nearest NaI detectors and one BGO detector. This package includes various spectral models, such as blackbody, BAND (Band et al. 1993), BAND+blackbody, power-law (PL), PL+blackbody, exponential cutoff power-law (CPL), and CPL+blackbody. The Bayesian information criterion (BIC) is used to indicate the goodness of fits to these models, where $2 \leqslant \Delta{\rm BIC} < 6$ gives positive evidence and $\Delta{\rm BIC} \geqslant 6$ gives strong positive evidence in favor of the model with a lower BIC (Kass & Raftery 1995). Here we adopt $\Delta{\rm BIC} = 6$ to select the best-fit model, and for those with $\Delta{\rm BIC} < 6$, we show two favored models. The main features, including the duration and best-fitting spectral models of the precursor and main SGRB emission components, are listed in Table 1. Figure 2 shows the statistics of the durations. We find that in most cases, the spectral models of both the precursor and the main SGRB can be constrained, while in four cases (GRB170802638, GRB180511437, GRB181126413, and GRB191221802), only the spectral models of the main SGRB can be constrained. Most precursors can be fitted by the blackbody, PL or CPL models with $\Delta{\rm BIC} \gtrsim 2$. Note for GRB081216531, although both blackbody and CPL models are favored with $\Delta{\rm BIC} = 5.9$, the spectral index of CPL ($N(E) \propto E^{2.1}$) would suggest a blackbody origin. Three typical precursor spectra are shown in Figures 3–5 as examples. The best-fitting models for the main SGRBs are usually CPL or BAND models with $\Delta{\rm BIC} \gtrsim 2$, but some can be fitted with the blackbody, PL, or CPL+blackbody models. Most precursors have different spectra from the main SGRBs, except GRB160804180 (both are CPL or BAND models) and GRB170709334 (both are blackbody or CPL models).

In the top panels of Figure 2, we show the histograms of $T_{\rm pre}$, $T_{\rm wt}$, and $T_{\rm GRB}$. In the bottom panels, we directly compare these three timescales in scatterplots. One can see that $T_{\rm wt} \sim T_{\rm GRB} \sim T_{\rm pre}$ is generally satisfied. The differential number distributions of $T_{\rm pre}$ and $T_{\rm wt}$ seem to be consistent with normal distributions, but more data are required to draw a firmer conclusion. The precursor component has a typical duration of $T_{\rm pre} \lesssim 0.7$ s, with a significant outlier GRB180511437 that has $T_{\rm pre} \approx 2.8$ s. In most cases, the waiting time satisfies $T_{\rm wt} < 2$ s, but there are two significant outliers: GRB180511437 with $T_{\rm wt} \approx 13$ s and GRB191221802 with $T_{\rm wt} \approx 19$ s. Using the linear regression method, we find a linear correlation in logarithmic scale, i.e., $T_{\rm wt} \approx 2.8\ T_{\rm GRB}^{1.2}$, with the correlation coefficient being $r = 0.75$. However, there is also an outlier, GRB191221802, with $T_{\rm wt}/T_{\rm GRB} \approx 52$.

3. Physical Implications for Precursor Emission in SGRBs

It has been argued that the classification of SGRBs based on T_{90} could be biased for some GRBs, especially those at high redshifts (e.g., $z \gtrsim 1$). These apparent SGRBs could be

Table 1
The SGRBs with Precursor Emission and Their Properties

Name[a]	$T_{\rm pre}$ (s)	Best-fit Models of Precursors[b] Energy Unit (keV)	ΔBIC	$T_{\rm wt}$ (s)	$T_{\rm GRB}$ (s)	Best-fit Model of Main Pulse[a] Energy Unit (keV)	ΔBIC	f-factor
GRB081216531	$0.15^{+0.05}_{-0.03}$	Blackbody: $kT = 18.66^{+3.30}_{-2.11}$; CPL: $\Gamma_{\rm ph} = 2.1^{+1.20}_{-1.73}$, $E_p = 72.49^{+17.17}_{-8.61}$	⩾5.9	$0.53^{+0.04}_{-0.05}$	$0.24^{+0.02}_{-0.02}$	CPL + Blackbody: $\Gamma_{\rm ph} = 0.08^{+0.27}_{-0.03}$, $E_p = 265.94^{+36.65}_{-30.44}$, $kT = 340.85^{+31.98}_{-21.47}$; CPL: $\Gamma_{\rm ph} = -0.50^{+0.06}_{-0.06}$, $E_p = 1219.0^{+103.1}_{-114.5}$	⩾5.0	2.0 ± 0.1
GRB090510016[*,c]	$0.05^{+0.07}_{-0.03}$	Blackbody: $kT = 120.43^{+103.18}_{-56.11}$; PL: $\Gamma_{\rm ph} = -1.13^{+1.89}_{-4.19}$	⩾3.0	$0.52^{+0.04}_{-0.08}$	$0.30^{+0.01}_{-0.01}$	CPL: $\Gamma_{\rm ph} = -0.61^{+0.03}_{-0.02}$, $E_p = 2999.44^{+0.55}_{-62.77}$	⩾79.7	2.6 ± 1.0
GRB100223110	$0.02^{+0.03}_{-0.01}$	Blackbody: $kT = 66.02^{+135.35}_{-15.62}$; PL: $\Gamma_{\rm ph} = -1.17^{+0.09}_{-4.01}$	⩾1.7	$0.08^{+0.02}_{-0.03}$	$0.12^{+0.01}_{-0.01}$	CPL: $\Gamma_{\rm ph} = -0.18^{+0.11}_{-0.12}$, $E_p = 1101.63^{+181.12}_{-107.93}$; BAND: $\alpha = -0.19^{+0.12}_{-0.11}$,$\beta = -13.65^{+7.55}_{-3.52}$, $E_p = 1122.3^{+153.4}_{-123.9}$	⩾5.8	1.4 ± 0.1
GRB100827455	$0.11^{+0.05}_{-0.04}$	Blackbody: $kT = 98.60^{+145.67}_{-37.80}$; PL: $\Gamma_{\rm ph} = -1.47^{+0.14}_{-3.74}$	⩾4.1	$0.34^{+0.06}_{-0.06}$	$0.09^{+0.02}_{-0.01}$	Blackbody: $kT = 168.19^{+82.07}_{-57.24}$; PL: $\Gamma_{\rm ph} = -1.11^{+0.17}_{-3.74}$;	⩾1.7	1.4 ± 0.3
GRB101208498	$0.17^{+0.12}_{-0.08}$	Blackbody: $kT = 9.74^{+1.90}_{-1.68}$; PL: $\Gamma_{\rm ph} = -2.20^{+0.20}_{-0.44}$;	⩾1.1	$1.17^{+0.10}_{-0.14}$	$1.03^{+0.03}_{-0.04}$	CPL: $\Gamma_{\rm ph} = -0.77^{+0.06}_{-0.07}$, $E_p = 148.24^{+9.76}_{-6.77}$; BAND: $\alpha = -0.67^{+0.17}_{-0.17}$, $\beta = -2.63^{+0.34}_{-14.26}$, $E_p = 127.6^{+29.4}_{-15.9}$	⩾3.8	3.6 ± 0.2
GRB111117510[*]	$0.18^{+0.05}_{-0.03}$	CPL: $\Gamma_{\rm ph} = -0.47^{+0.22}_{-0.32}$, $E_p = 576.84^{+442.45}_{-91.69}$;	⩾6.0	$0.22^{+0.03}_{-0.06}$	$0.09^{+0.01}_{-0.01}$	Blackbody: $kT = 55.31^{+10.38}_{-6.86}$; CPL: $\Gamma_{\rm ph} = -0.02^{+0.70}_{-0.48}$, $E_p = 254.25^{+104.53}_{-39.43}$	⩾2.1	1.3 ± 0.1
GRB140209313[*,d]	$0.61^{+0.08}_{-0.08}$	CPL: $\Gamma_{\rm ph} = -1.07^{+0.92}_{-0.60}$, $E_p = 114.74^{+1526.38}_{-49.19}$; PL: $\Gamma_{\rm ph} = -1.74^{+0.06}_{-0.10}$	⩾2.3	$1.10^{+0.08}_{-0.08}$	$1.03^{+0.04}_{-0.06}$	BAND: $\alpha = -0.31^{+0.06}_{-0.05}$, $\beta = -2.44^{+0.07}_{-0.08}$, $E_p = 139.66^{+6.33}_{-5.77}$;	⩾61.9	7.3 ± 0.6
GRB141102536[*]	$0.06^{+0.10}_{-0.06}$	Blackbody: $kT = 83.92^{+38.77}_{-12.07}$;	⩾6.0	$1.26^{+0.11}_{-0.15}$	$0.48^{+0.04}_{-0.04}$	CPL: $\Gamma_{\rm ph} = -0.52^{+0.15}_{-0.15}$, $E_p = 402.76^{+88.86}_{-46.93}$; BAND: $\alpha = -0.53^{+0.14}_{-0.16}$,$\beta = -3.53^{+1.19}_{-13.6}$, $E_p = 405.9^{+91.9}_{-48.8}$	⩾5.7	1.6 ± 0.1
GRB150604434	$0.17^{+0.25}_{-0.01}$	Blackbody: $kT = 124.78^{+31.32}_{-17.16}$; CPL: $\Gamma_{\rm ph} = 0.04^{+0.79}_{-0.40}$, $E_p = 637.59^{+260.37}_{-142.66}$	⩾3.1	$0.64^{+0.02}_{-0.29}$	$0.21^{+0.03}_{-0.02}$	CPL: $\Gamma_{\rm ph} = -0.35^{+0.24}_{-0.28}$, $E_p = 414.84^{+198.21}_{-73.32}$; BAND: $\alpha = -0.13^{+0.08}_{-0.49}$, $\beta = -2.25^{+0.31}_{-14.98}$, $E_p = 293.4^{+310.1}_{-95.8}$	⩾5.4	1.5 ± 0.1
GRB150922234	$0.05^{+0.01}_{-0.01}$	PL: $\Gamma_{\rm ph} = -1.91^{+0.35}_{-2.85}$; Blackbody: $kT = 7.65^{+212.99}_{-5.99}$	⩾2.2	$0.03^{+0.01}_{-0.01}$	$0.08^{+0.01}_{-0.01}$	CPL: $\Gamma_{\rm ph} = -0.23^{+0.21}_{-0.17}$, $E_p = 474.00^{+86.67}_{-64.00}$; CPL + Blackbody: $\Gamma_{\rm ph} = 0.37^{+1.13}_{-0.30}$, $E_p = 651.1^{+85.2}_{-429.2}$, $kT = 39.63^{+463.1}_{-37.5}$	⩾4.8	1.3 ± 0.1
GRB160804180	$0.16^{+0.02}_{-0.02}$	CPL: $\Gamma_{\rm ph} = -0.46^{+0.21}_{-0.41}$, $E_p = 343.30^{+292.95}_{-58.10}$; BAND: $\alpha = -0.54^{+0.31}_{-0.35}$, $\beta = -18.57^{+13.64}_{-1.41}$, $E_p = 359.4^{+312.0}_{-78.5}$	⩾5.9	$0.17^{+0.02}_{-0.02}$	$0.26^{+0.02}_{-0.02}$	CPL: $\Gamma_{\rm ph} = -0.24^{+0.17}_{-0.19}$, $E_p = 619.80^{+163.11}_{-77.88}$; BAND: $\alpha = -0.23^{+0.16}_{-0.20}$, $\beta = -19.55^{+13.61}_{-0.45}$, $E_p = 623.6^{+153.9}_{-83.5}$	⩾5.9	1.6 ± 0.1
GRB170709334	$0.46^{+0.01}_{-0.27}$	Blackbody: $kT = 62.44^{+23.18}_{-7.05}$; CPL: $\Gamma_{\rm ph} = -0.52^{+1.92}_{-0.23}$, $E_p = 723.04^{+453.48}_{-460.33}$	⩾5.1	$0.17^{+0.30}_{-0.07}$	$0.15^{+0.07}_{-0.04}$	Blackbody: $kT = 88.49^{+16.88}_{-10.64}$; CPL: $\Gamma_{\rm ph} = 0.63^{+0.82}_{-0.58}$, $E_p = 380.01^{+119.84}_{-54.90}$	⩾4.4	1.3 ± 0.1
GRB170802638	$0.15^{+0.17}_{-0.11}$	unconstrained		$1.85^{+0.14}_{-0.21}$	$0.33^{+0.04}_{-0.04}$	CPL: $\Gamma_{\rm ph} = -0.62^{+0.07}_{-0.09}$, $E_p = 799.50^{+155.17}_{-85.57}$; CPL + Blackbody: $\Gamma_{\rm ph} = 0.01^{+0.17}_{-0.01}$, $E_p = 269.3^{+24.9}_{-36.5}$, $kT = 339.0^{+65.6}_{-51.9}$	⩾5.5	1.5 ± 0.1
GRB180511437	$2.80^{+1.38}_{-1.69}$	unconstrained		$12.72^{+1.80}_{-1.57}$	$3.33^{+0.18}_{-0.24}$	CPL: $\Gamma_{\rm ph} = -0.81^{+0.22}_{-0.27}$, $E_p = 119.70^{+31.63}_{-15.83}$; BAND: $\alpha = -0.413^{+0.41}_{-0.65}$, $\beta = -2.68^{+0.51}_{-14.44}$, $E_p = 87.1^{+60.7}_{-13.4}$	⩾5.5	1.4 ± 0.1
GRB181126413[*]	$0.72^{+0.18}_{-0.27}$	unconstrained		$0.85^{+0.40}_{-0.29}$	$0.46^{+0.11}_{-0.13}$	Blackbody: $kT = 24.52^{+3.16}_{-2.04}$;	⩾6.2	1.2 ± 0.1
GRB191221802	$0.03^{+0.59}_{-0.03}$	unconstrained		$19.36^{+1.24}_{-3.19}$	$0.37^{+0.26}_{-0.13}$	Blackbody: $kT = 67.21^{+22.62}_{-9.46}$;	⩾1.0	1.1 ± 0.1

Table 1
(Continued)

Name[a]	$T_{\rm pre}$ (s)	Best-fit Models of Precursors[b] Energy Unit (keV)	ΔBIC	$T_{\rm wt}$ (s)	$T_{\rm GRB}$ (s)	Best-fit Model of Main Pulse[a] Energy Unit (keV)	ΔBIC	f-factor
						CPL: $\Gamma_{\rm ph} = -0.57^{+0.48}_{-0.53}$, $E_p = 471.92^{+945.05}_{-126.29}$;		

Notes. The durations of the precursor ($T_{\rm pre}$), waiting time ($T_{\rm wt}$), and the main SGRB ($T_{\rm GRB}$) are based on T_{90} analyses. The best-fit models are obtained with the BIC.

[a] The GRBs marked with "*" also triggered Swift, and can be found at https://swift.gsfc.nasa.gov/archive/grb_table/.

[b] For the blackbody model, k and T are the Boltzmann constant and temperature, respectively. PL ($N(E) \propto E^{\Gamma_{\rm ph}}$) and CPL ($N(E) \propto E^{\Gamma_{\rm ph}} \exp[-E(2+\Gamma_{\rm ph})/E_p]$) represent power-law and cutoff power-law models with photon indices $\Gamma_{\rm ph}$, and E_p is the peak energy for the CPL model. For those unconstrained events, we find that both blackbody and PL models are favored, but there are too few photons to provide a robust constraint on the parameters. The ΔBIC between the best-fit model and other models are also presented. And for ΔBIC < 6, two favored models are provided.

[c] The redshift of GRB090510016 is 0.903 (Rau et al. 2009). Troja et al. (2010) found there are two precursors in this burst from the Swift data.

[d] From the Swift observation, GRB140209313 was found to be an SGRB with extended emission, which has durations of $T_{90} = 21.25 \pm 7.98$ s and $T_{50} = 0.61 \pm 0.07$ s, respectively (Palmer et al. 2014).

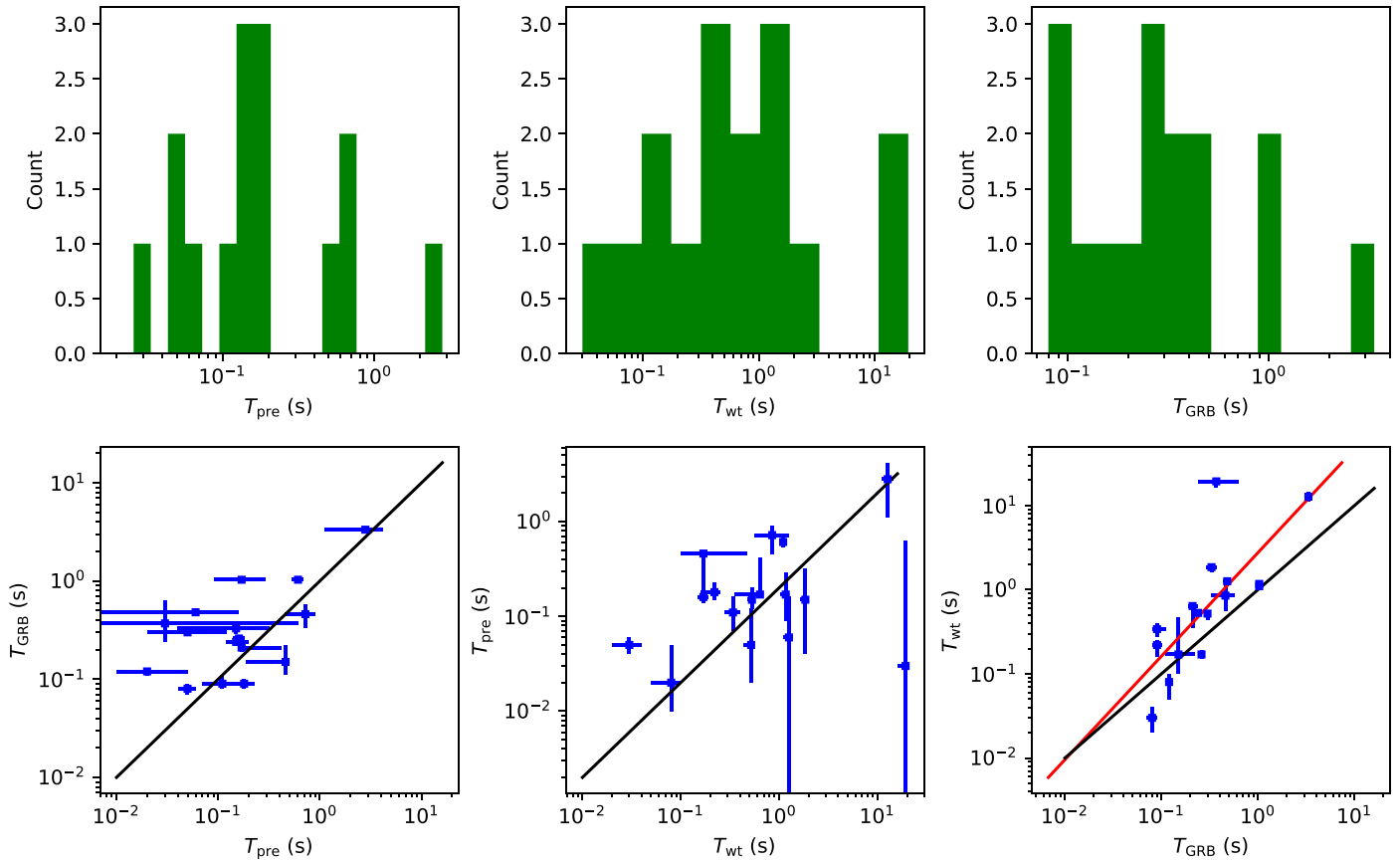

Figure 2. The top panels show the histograms of T_{pre}, T_{wt}, and T_{GRB}. The bottom panels show comparisons of these timescales, and the black lines represent the equality line. The red line in the right bottom panel is $T_{wt} \approx 2.8\ T_{GRB}{}^{1.2}$.

intrinsically from collapsars, yet the observed light curve is just the "tip-of-iceberg" (e.g., Zhang et al. 2009; Virgili et al. 2011; Bromberg et al. 2013; Lü et al. 2014) of the emission with a longer duration. In our sample, the redshift of most events is unknown, except GRB090510016, which has a spectroscopic redshift $z = 0.903$ (Rau et al. 2009). Therefore, we calculate the amplitude f-factor for these SGRBs (see more details in Lü et al. 2014) to determine the probability of some of them might be disguised SGRBs. We find that eight (four) of them have $f \gtrsim 1.5$ (2), as listed in Table 1. These numbers are large enough to support their NS merger origins (Lü et al. 2014). In the following, we mainly discuss the precursor models based on the NS merger scenario, keeping in mind that in rare cases, a collapsar origin of the SGRB cannot be ruled out.

3.1. Precursor Models

Within the framework of NS mergers, several scenarios have been discussed in the literature that may give rise to precursor emission before the main SGRB. We discuss four possibilities below. The first two are pre-merger models and the last two are post-merger models.

1. *The pre-merger NS crust-cracking model*: For this mechanism, the dissipated energy likely is emitted in thermal radiation, since the crust is highly optically thick. The energy released in this process is found to be $E_{cc,46} = E_{cc}/10^{46}\,\mathrm{erg} \lesssim 1$ (Troja et al. 2010; Tsang et al. 2012). This would heat the crust to $T_c = E_{cc}/C \lesssim 2.8 \times 10^8$ K, where $C \approx 10^{29} T_c$ erg K^{-1} (Yakovlev et al. 1999). The corresponding luminosity from the crust surface is
$$L_{cc} \approx 4\pi R_*^2 a T_c^4 \lesssim 4.5 \times 10^{42} E_{cc,46}^2\ \mathrm{erg\ s^{-1}}, \quad (1)$$
where a is the Stefan–Boltzmann constant, and the NS radius is assumed to be $R_* = 10^6$ cm.
2. *The pre-merger magnetosphere interaction model*: The luminosity of magnetospheric interaction between two NSs can be estimated as (Lai 2012; Palenzuela et al. 2013; Wang et al. 2018b)
$$L_{MI} \approx 2.0 \times 10^{46} \eta B_{*,13}^2 (a/30\ \mathrm{km})^{-7}\ \mathrm{erg\ s^{-1}}, \quad (2)$$
where $B_* = 10^{13} B_{*,13}$ G is the magnetic field of the main NS, a is the separation between the two NSs, and the efficiency parameter $0.01 \lesssim \eta \lesssim 1$ depends on the magnetic field structure of the binary system.
3. *The post-merger shock breakout (SBO) model*: The SBO of the jet or cocoon from the fast component of the NS merger ejecta can release a minute fraction ($\zeta = 10^{-4}\zeta_{-4}$) of the total kinetic energy of the outflow, i.e., $E_{SBO} = \zeta E_{iso}$ (Bromberg et al. 2018; Gottlieb et al. 2018). The luminosity of an SBO may be estimated as
$$L_{SBO} \approx E_{SBO}/t_{SBO} = 10^{47} \zeta_{-4} L_{j,50} T_{GRB} t_{SBO,-1}^{-1}\ \mathrm{erg\ s^{-1}}, \quad (3)$$
where we used $E_{iso} = L_j T_{GRB}$, and $L_j = 10^{50} L_{j,50}$ erg s^{-1} is the isotropic-equivalent jet luminosity. The SBO takes place at a radius of $R_{SBO} \approx \Gamma_{SBO}^2 c t_{SBO}$, where Γ_{SBO} is the Lorentz factor of the emitting region, which is $\Gamma_{SBO} \sim 10$ for jet breakout and $\Gamma_{SBO} \sim 3$ for cocoon

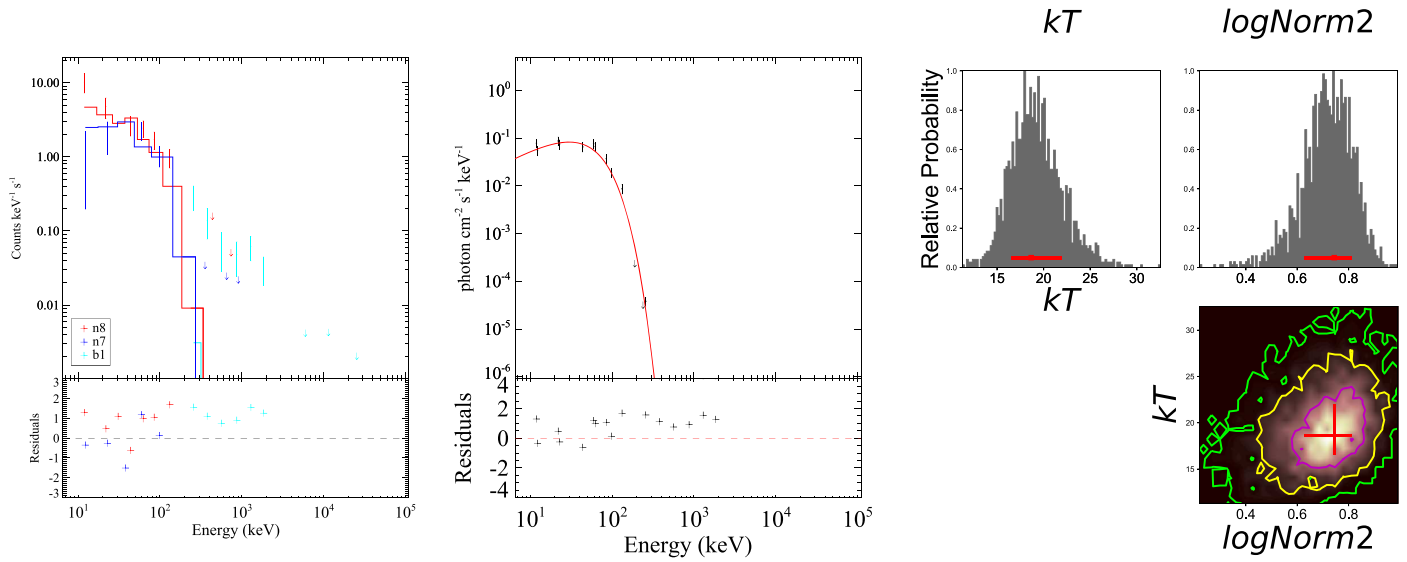

Figure 3. Constraints on the blackbody model of the precursor of GRB081216531.

breakout; $t_{\rm SBO} = 0.1 t_{\rm SBO,-1}$ s is the SBO timescale; The observed spectrum is quasi-thermal with a temperature $T_{\rm SBO} \sim \Gamma_{\rm SBO}$(1–50) keV (Bromberg et al. 2018; Gottlieb et al. 2018).

4. *The post-merger fireball photosphere model*: The luminosity of photospheric radiation of a GRB fireball can be expressed as

$$L_{\rm ph} = 10^{50} \xi L_{\rm j,50}\ {\rm erg\ s^{-1}}, \quad (4)$$

where $\xi = \min[1, (R_{\rm c}/R_{\rm ph})^{2/3}]$ with $R_{\rm c}$ and $R_{\rm ph}$ being the coasting radius and photosphere radius, respectively (see Section 7.3.3 of Zhang 2018, and references therein). This leads to a quasi-blackbody spectrum with a temperature

$$kT_{\rm ph} = \xi kT_0 = 40.9 \xi_{-1} L_{\rm j,50}^{1/4} R_{0,7}^{-1/2}\ {\rm keV}, \quad (5)$$

where T_0 and $R_0 = 10^7 R_{0,7}$ cm are the initial temperature and the size of the fireball.

Recently, Dichiara et al. (2020) performed a systematic search for SGRBs in the local universe based on the Swift catalog, and found that the four closest SGRBs could be located at distances of 100–200 Mpc. The sensitivity of Fermi/GBM is roughly 0.5 cm^{-2} s^{-1} assuming a photon energy of 100 keV.[7] The corresponding threshold luminosity for the events detectable at a luminosity distance of $D > 100$ Mpc is

$$L_{\rm th} \sim 10^{47}\ {\rm erg\ s^{-1}} (D/100\ {\rm Mpc})^2. \quad (6)$$

Comparing this with the predicted luminosities of the four precursor models, one can see that the crust-cracking model predicts too faint precursor emission to be detectable. For cosmological-distance SGRBs ($D > 100$ Mpc), only the SBO emission and fireball photosphere model can give rise to a bright enough precursor for SGRBs. The magnetosphere interaction model may be relevant to precursor emission of some SGRBs if the sources are nearby and the surface magnetic field of the primary NS is strong enough (e.g., $B_s > 10^{13}$ G).

[7] See https://fermi.gsfc.nasa.gov/science/instruments/table1-2.html.

3.2. Constraints on GRB Models

Some precursors in our sample can be explained by the blackbody model with $\Delta{\rm BIC} \gtrsim 2$, especially GRB081216531 and GRB141102536 with $\Delta{\rm BIC} \gtrsim 6$ (see Table 1). This is consistent with the SBO and fireball photosphere model. The observed relative flux ratio between the precursor and the main SGRB is about $0.01 \lesssim L_{\rm pre}/L_{\rm j} < 1$ in our sample. For the SBO model, it requires $10 \lesssim \zeta_{-4} T_{\rm GRB} t_{\rm SBO,-1}^{-1} < 10^3$.

For the fireball photosphere model, the relative flux ratio as well as the precursor temperature can be well explained by the model with $1 > \xi \gtrsim 0.01$. The observed duration of the photospheric radiation is characterized by $t_{\rm ph} \approx R_{\rm ph}(1+z)/(\Gamma^2 c)$, where z is the redshift, Γ is the bulk Lorentz factor of the jet, and the photosphere radius is $R_{\rm ph} = 5.9 \times 10^{13} L_{\rm j,50} \Gamma_1^{-3}$ cm, where $\Gamma_1 = \Gamma/10$ (e.g., Mészáros & Rees 2000; Rees & Mészáros 2005; Zhang 2018). Our sample shows that $t_{\rm ph} \approx 0.1 t_{\rm ph,-1}$ s, which gives an interesting constraint on the bulk Lorentz factor of SGRB outflow, i.e.,

$$\Gamma = 28.8 L_{\rm j,50}^{1/5} t_{\rm ph,-1}^{-1/5}. \quad (7)$$

This result is consistent with Equation (1) of Troja et al. (2010). Note this interpretation requires a matter-dominated jet, with the main SGRB signal originating from internal shocks (Mészáros & Rees 2000; Zhang 2018).

For the post-merger precursor models, the waiting time between the precursor and the main burst corresponds to the observer-frame time for the jet to propagate from the precursor radius $R_{\rm pre}$ (photospheric radius or SBO radius) to the jet dissipation radius $R_{\rm GRB}$, i.e., $T_{\rm wt} = (R_{\rm GRB} - R_{\rm pre})(1+z)/(\Gamma^2 c)$. Observations show $T_{\rm wt} \sim T_{\rm pre}$ (see Figure 2), which indicates that $R_{\rm GRB} \sim 2R_{\rm ph}$ for the fireball photosphere model, and $R_{\rm GRB} \sim \Gamma^2 \Gamma_{\rm SBO}^{-2} R_{\rm SBO}$ for the SBO model. However, we should keep in mind that the definition of $T_{\rm pre}$ and $T_{\rm GRB}$ here are based on T_{90}, which could underestimate the intrinsic durations of the precursor and the main burst and overestimate the waiting time. The main GRB signal is expected be nonthermal, which is consistent with our spectral fits for most events. One exception is GRB170709334, which favors thermal spectra for both the precursor and the main GRB. This may correspond to an SBO precursor with a

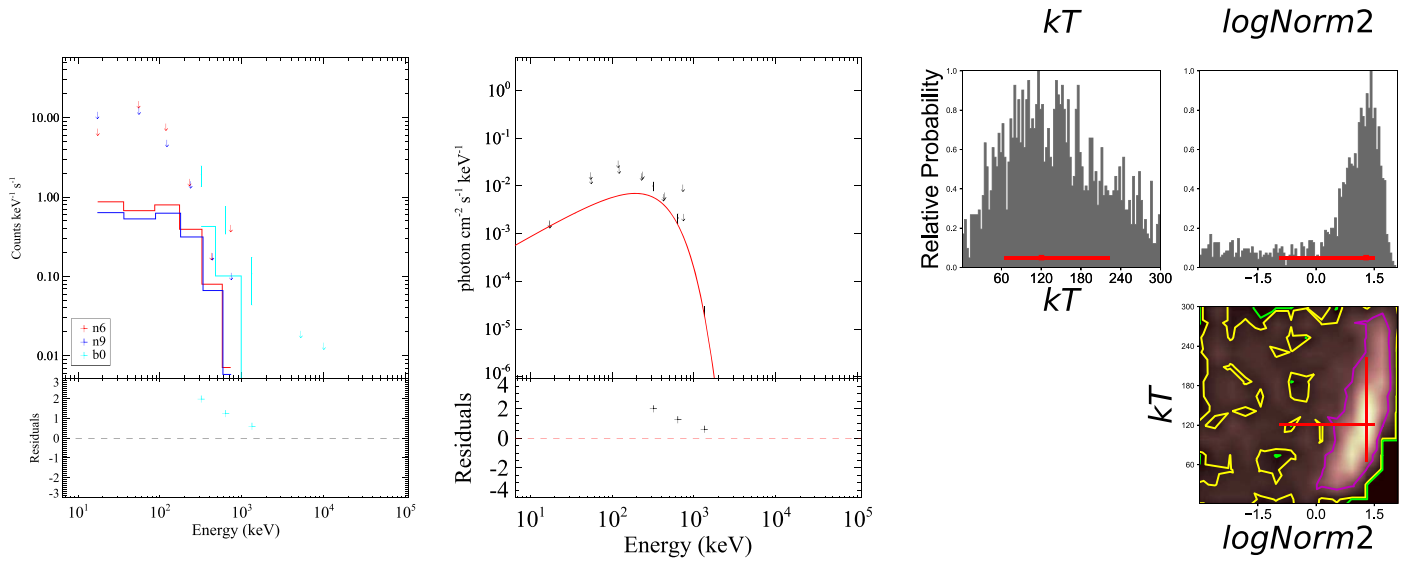

Figure 4. Constraints on the blackbody model of the precursor of GRB090510016.

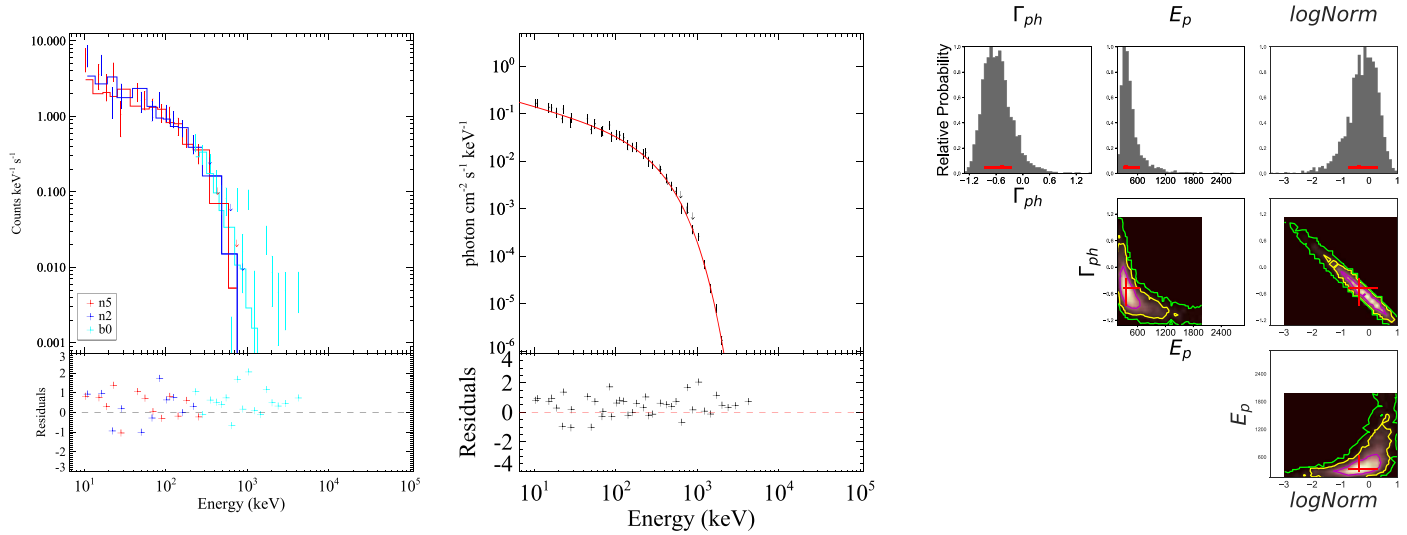

Figure 5. Constraints on the CPL model of the precursor of GRB160804180.

fireball-photosphere-induced main pulse or two episodes of central engine activities with the internal shock emission suppressed.

In some cases, the precursor emission has a nonthermal spectrum, especially GRB111117510 and GRB160804180 with $\Delta\mathrm{BIC} \gtrsim 6$. These cases may be explained by the NS magnetospheric interaction model (assuming that the sources are nearby). For NS mergers with the surface magnetic field $B_{*,13} \gtrsim 1$ for the primary NS, the typical spectrum may be approximately described by a synchrotron radiation spectrum of a photon index around $-2/3$ peaking at ~MeV, because of the effect of synchrotron-pair cascades (Wang et al. 2018a, 2018b). Such a model can well explain the photon indices and peak energies of the nonthermal precursor bursts, e.g., GRB111117510, GRB140209313, and GRB160804180 (Wang et al. 2018b). The precursor emission time for this magnetospheric interaction model roughly coincides with the gravitational-wave radiation chirp signal time. So the waiting time between the precursor and the main burst should correspond to the time delay between the GW signal and the SGRB signal. This timescale consists of three parts (Zhang 2019): the time ($\Delta t_{\rm jet}$) for the jet to be launched by the central engine, the time ($\Delta t_{\rm bo}$) for the jet to propagate through and break out from the circumburst medium, and the time ($\Delta t_{\rm GRB}$) for the jet to reach the energy dissipation radius (e.g., the photospheric radius or the internal shock radius). The last term is $\Delta t_{\rm GRB}/(1+z) \sim T_{\rm GRB}/(1+z) \sim 0.01-1$ s, while the first two terms depend on the jet-launch models. According to the Table 1 in Zhang (2019), for most models, $(\Delta t_{\rm jet}+\Delta t_{\rm bo})/(1+z) = 0.01$–1 s. Consequently, one would also expect $T_{\rm wt} \sim T_{\rm GRB}$. An exception is the SMNS/SNS magnetic model, in which a uniform-rotation-supported supramassive NS (SMNS) is formed after the NS merger, which subsequently becomes a stable NS (SNS). In this model, the waiting time is dominated by the term $\Delta t_{\rm jet}/(1+z) = 0.01-10$ s, which is mainly contributed by the time needed to clean the environment to launch a relativistic jet (Metzger et al. 2011; Zhang 2019). In this case, one expects $T_{\rm wt} \gg T_{\rm GRB}$. In our sample, we find most events satisfy $T_{\rm wt} \sim T_{\rm GRB}$, except GRB191221802, which has $T_{\rm wt}/T_{\rm GRB} \approx 52$ and $T_{\rm wt} = 19.36^{+1.24}_{-3.19}$ s. We also notice that for GRB090510016, Troja et al. (2010) found two precursors in the Swift data, but only the second precursor can be found in Fermi data (consistent with

our results). Its first precursor is found to be of $T_{\rm wt}/T_{\rm GRB} \approx 40$ and $T_{\rm wt} \approx 12$ s, while its second precursor in our analysis is consistent with the photospheric radiation of the fireball. Therefore, its first precursor with a long waiting time ($T_{\rm wt}/T_{\rm GRB} \gg 1$) could originate from NS magnetospheric interaction, and such long waiting times are caused by the jet-launch mechanism in the SMNS/SNS magnetic model. In conclusion, according to this model, an SNS engine might have been formed after the merger in events with $T_{\rm wt}/T_{\rm GRB} \gg 1$, e.g., GRB090510016 and GRB191221802.

4. Conclusions and Discussion

In this Letter, we performed a stringent search for precursor emission of short GRBs in the Fermi/GBM data and found that 16 out of 529 (3.0%) SGRBs have precursor with significance $\gtrsim 4.5\sigma$. The light curves are shown in Figure 1, and the properties of precursor and main SGRB emission are listed in Table 1. As shown in Figure 2, the timescales are roughly comparable to each other, $T_{\rm wt} \sim T_{\rm GRB} \sim T_{\rm pre}$, and there is a linear correlation (correlation coefficient $r = 0.75$) $T_{\rm wt} \approx 2.8\, T_{\rm GRB}^{1.2}$ in the logarithmic scale, but with a significant outlier $T_{\rm wt}/T_{\rm GRB} \approx 52$ in GRB191221802. In most cases, we find $T_{\rm pre} \lesssim 0.7$ s and $T_{\rm wt} < 2$ s, but there are significant outliers, i.e., $T_{\rm pre} \approx 2.8$ s and $T_{\rm wt} \approx 13$ s for GRB180511437, and $T_{\rm wt} \approx 19$ s for GRB191221802.

Most precursors favor the blackbody, CPL, and/or PL spectra with $\Delta{\rm BIC} \gtrsim 2$. In particular, GRB081216531 and GRB141102536 favor the blackbody model with $\Delta{\rm BIC} \gtrsim 6$, and GRB111117510 and GRB160804180 favor the CPL model with $\Delta{\rm BIC} \gtrsim 6$. The thermal spectra can be explained within the SBO model and the photospheric radiation fireball model, and the nonthermal ones may be explained in the NS magnetospheric interaction model. The crust-cracking mechanisms generally predict too faint emission to be detected at a cosmological distance. For the SBO model, we constrain $10^{-2} T_{\rm GRB}/T_{\rm pre} \lesssim \zeta < 1$. This is larger than the expected value of $\zeta \sim 10^{-4}$–10^{-3} (Bromberg et al. 2018; Gottlieb et al. 2018). One possible explanation is that the jet is viewed slightly off-axis so that the observed luminosity of the main pulse is smaller than the jet luminosity. For the photospheric radiation mechanism, a matter-dominated jet is preferred. We constrain the jet Lorentz factor to be $\Gamma = 28.8 L_{\rm j,50}^{1/5} t_{\rm ph,-1}^{-1/5}$. However, as noted by Troja et al. (2010), such a Lorentz factor is much smaller than that of typical SGRBs and thus may have difficulties explaining SGRB properties. For example, observation shows that the Lorentz factor of GRB090510016 should be $\Gamma \gtrsim 10^3$ (Ackermann et al. 2010). For the NS magnetospheric interaction model, we find it can provide a constraint on the jet-launch mechanism. More specifically, we find events with $T_{\rm wt}/T_{\rm GRB} \gg 1$ can be well explained by the time delay to launch a relativistic jet in the SMNS/SNS magnetic model. As a consequence, in GRB191221802 there might be an SNS formed after each merger, and their jets are magnetically powered.

We also notice that the possibility that some events in our sample are from collapsars cannot be excluded. For example, it is unclear whether GRB180511437 is a short GRB or not, as our study shows $T_{\rm GRB} = 3.33^{+0.18}_{-0.24}$ s, which is >2 s, even though it has $T_{\rm GRB} = 1.98 \pm 0.97$ in the Fermi GBM Burst Catalog.[8] Besides, the precursor of GRB160804180 can be also explained by the BAND model with $\Delta{\rm BIC} = 5.9$, which might be an early episode activity from the central engine. Furthermore, it is also suggested that GRB090510016 could be of collapsar origin based on the study of its afterglow (Zhang et al. 2009; Panaitescu 2011). Such gray-zone cases can be better studied when multiwavelength/multimessenger information (e.g., host galaxy identifications) becomes available (e.g., Dichiara et al. 2020; Li et al. 2020).

Albeit only 3.0% of SGRBs detected by Fermi/GBM have detectable precursor emission, we note that the opening angles of precursors from SBOs (especially for cocoon breakouts) and NS magnetospheric interactions can have a solid angle much larger than the jet opening angle. Therefore, searching EM counterparts of NS mergers in the local universe will very likely detect such precursor emissions with/without detecting the main SGRBs. GW170817/GRB 170817A may be such a case.

We thank the referee for valuable comments. J.S.W. is supported by China Postdoctoral Science Foundation (grants 2018M642000, 2019T120335). B.B.Z. acknowledges the support by the Fundamental Research Funds for the Central Universities (14380035). This work is also supported by National Key Research and Development Programs of China (2018YFA0404204) and The National Natural Science Foundation of China (grant No. 11833003).

Software: McSpecFit; Astropy.

ORCID iDs

Jie-Shuang Wang https://orcid.org/0000-0002-2662-6912
Bin-Bin Zhang https://orcid.org/0000-0003-4111-5958
Bing Zhang https://orcid.org/0000-0002-9725-2524

References

Abbott, B. P., Abbott, R., Abbott, T. D., et al. 2017a, PhRvL, 119, 161101
Abbott, B. P., Abbott, R., Abbott, T. D., et al. 2017b, ApJL, 848, L13
Abbott, B. P., Abbott, R., Abbott, T. D., et al. 2020, ApJL, 892, L3
Ackermann, M., Asano, K., Atwood, W. B., et al. 2010, ApJ, 716, 1178
Astropy Collaboration, Price-Whelan, A. M., Sipőcz, B. M., et al. 2018, AJ, 156, 123
Band, D., Matteson, J., Ford, L., et al. 1993, ApJ, 413, 281
Berger, E. 2014, ARA&A, 52, 43
Bromberg, O., Nakar, E., Piran, T., & Sari, R. 2013, ApJ, 764, 179
Bromberg, O., Tchekhovskoy, A., Gottlieb, O., Nakar, E., & Piran, T. 2018, MNRAS, 475, 2971
Burlon, D., Ghirlanda, G., Ghisellini, G., et al. 2008, ApJL, 685, L9
Burlon, D., Ghirlanda, G., Ghisellini, G., Greiner, J., & Celotti, A. 2009, A&A, 505, 569
Dichiara, S., Troja, E., O'Connor, B., et al. 2020, MNRAS, 492, 5011
Fernández, R., & Metzger, B. D. 2016, ARNPS, 66, 23
Geng, J.-J., Zhang, B., Kölligan, A., Kuiper, R., & Huang, Y.-F. 2019, ApJL, 877, L40
Gill, R., Nathanail, A., & Rezzolla, L. 2019, ApJ, 876, 139
Goldstein, A., Hamburg, R., Wood, J., et al. 2019, arXiv:1903.12597
Goldstein, A., Veres, P., Burns, E., et al. 2017, ApJL, 848, L14
Gottlieb, O., Nakar, E., Piran, T., & Hotokezaka, K. 2018, MNRAS, 479, 588
Hansen, B. M. S., & Lyutikov, M. 2001, MNRAS, 322, 695
Hu, Y.-D., Liang, E.-W., Xi, S.-Q., et al. 2014, ApJ, 789, 145
Kass, R. E., & Raftery, A. E. 1995, J. Am. Stat. Assoc., 90, 773
Lai, D. 2012, ApJL, 757, L3
Lazzati, D. 2005, MNRAS, 357, 722
Li, Y., Zhang, B., & Yuan, Q. 2020, ApJ, 897, 154
Lü, H.-J., Zhang, B., Liang, E.-W., Zhang, B.-B., & Sakamoto, T. 2014, MNRAS, 442, 1922
Mészáros, P., & Rees, M. J. 2000, ApJ, 530, 292
Metzger, B. D. 2019, LRR, 23, 1

[8] Can be accessed via https://heasarc.gsfc.nasa.gov/db-perl/W3Browse/w3table.pl?tablehead=name%3Dfermigbrst&Action=More+Options.

Metzger, B. D., Giannios, D., Thompson, T. A., Bucciantini, N., & Quataert, E. 2011, MNRAS, 413, 2031
Minaev, P. Y., & Pozanenko, A. S. 2017, AstL, 43, 1
Mooley, K. P., Deller, A. T., Gottlieb, O., et al. 2018a, Natur, 561, 355
Mooley, K. P., Nakar, E., Hotokezaka, K., et al. 2018b, Natur, 554, 207
Narayana Bhat, P., Meegan, C. A., von Kienlin, A., et al. 2016, ApJS, 223, 28
Palenzuela, C., Lehner, L., Ponce, M., et al. 2013, PhRvL, 111, 061105
Palmer, D. M., Barthelmy, S. D., Baumgartner, W. H., et al. 2014, GCN, 15812, 1
Panaitescu, A. 2011, MNRAS, 414, 1379
Ramirez-Ruiz, E., MacFadyen, A. I., & Lazzati, D. 2002, MNRAS, 331, 197
Rau, A., McBreen, S., & Kruehler, T. 2009, GCN, 9353, 1
Rees, M. J., & Mészáros, P. 2005, ApJ, 628, 847
Ryan, G., van Eerten, H., Piro, L., & Troja, E. 2020, ApJ, 896, 166
Scargle, J. D., Norris, J. P., Jackson, B., & Chiang, J. 2013, ApJ, 764, 167
Suvorov, A. G., & Kokkotas, K. D. 2020, PhRvD, 101, 083002
Troja, E., Piro, L., van Eerten, H., et al. 2017, Natur, 551, 71
Troja, E., Rosswog, S., & Gehrels, N. 2010, ApJ, 723, 1711
Troja, E., van Eerten, H., Ryan, G., et al. 2019, MNRAS, 489, 1919
Tsang, D., Read, J. S., Hinderer, T., Piro, A. L., & Bondarescu, R. 2012, PhRvL, 108, 011102
Virgili, F. J., Zhang, B., O'Brien, P., & Troja, E. 2011, ApJ, 727, 109
Wang, J.-S., Liu, R.-Y., Aharonian, F., & Dai, Z.-G. 2018a, PhRvD, 97, 103016
Wang, J.-S., Peng, F.-K., Wu, K., & Dai, Z.-G. 2018b, ApJ, 868, 19
Wang, J.-S., Yang, Y.-P., Wu, X.-F., Dai, Z.-G., & Wang, F.-Y. 2016, ApJL, 822, L7
Yakovlev, D. G., Levenfish, K. P., & Shibanov, Y. A. 1999, PhyU, 42, 737
Yang, Y.-S., Zhong, S.-Q., Zhang, B.-B., et al. 2020, ApJ, 899, 60
Zhang, B. 2018, The Physics of Gamma-Ray Bursts (Cambridge: Cambridge Univ. Press)
Zhang, B. 2019, FrPhy, 14, 64402
Zhang, B., Zhang, B.-B., Virgili, F. J., et al. 2009, ApJ, 703, 1696
Zhang, B. B., Zhang, B., Castro-Tirado, A. J., et al. 2018a, NatAs, 2, 69
Zhang, B. B., Zhang, B., Sun, H., et al. 2018b, NatCo, 9, 447
Zhong, S.-Q., Dai, Z.-G., Cheng, J.-G., Lan, L., & Zhang, H.-M. 2019, ApJ, 884, 25